Green Synthesis of Oxygen-vacancy-rich NiV-LDH Photocatalyst for Enhancement of Photocatalytic H_2O_2 Production and Cr(VI) Detoxification

Preeti Prabha Sarangi, Jyotirmayee Sahu, Rasan Kumar Giri, and Kulamani Parida*

[a] Centre for Nano Science and Nano Technology, ITER, Siksha 'O' Anusandhan Deemed to be University, Bhubaneswar, Odisha, India, 751030

**Corresponding author*

***Corresponding Author's Email:** *kulamaniparida@soa.ac.in*

paridakulamani@yahoo.com

Tel. No.: +91-674-2351777 and Fax. +91-674-2350642

Contents

Chemical Requirement

$NiCl_2$,$6H_2O$, VCl_3, Cd $(NO_3)_2.4H_2O$, KI and Ammonium heptamolybdate were purchased from sigma Aldrich, India. Isopropyl alcohol (IPA), Silver Nitrate ($AgNO_3$), para-benzoquinone (p-BQ), citric acid (CA), methanol, tertiary butyl alcohol (TBA) and ethanol were procured from Merck, India.

Synthetic protocol for NiV-LDH Photocatalyst

It has been reported that, presence of equal amount of bivalent and trivalent metal causes the structural distortion due to excessive positive charge. Hence for the successful synthesis of LDH, the M^{II}/M^{III} ratio were optimized as 2:1, 3:1 and 4:1 in this work.[1,2,3] A series of Ni–V–CO_3^{2-} LDHs were synthesized via a facile reflux method, as illustrated schematically in Figure 1a. For the synthesis of the photocatalysts, $NiCl_2 \cdot 6H_2O$, VCl_3, and urea (V^{3+}: urea = 1:12) were dispersed in 50 mL of ultrapure water, and the pH was adjusted between 8-10. The resulting mixture was continuously stirred for 48 h at 110°C. Based on the molar ratios of Ni and V (2:1, 3:1, and 4:1), the synthesized products were designated as Ni_2V- LDHs (NV-2), Ni_3V- LDHs (NV-3), and Ni_4V-LDHs (NV-4), respectively. [4]

Material Characterisation

Physicochemical Characterisations Techniques

The crystalline phases of the synthesized NV photocatalyst were investigated by a powder X-ray diffractometer (Rigaku Miniflex X-ray diffraction instrument) equipped with Cu Kα-1 radiation (λ = 1.54 nm), which was performed at a scanning range of 5°–80°, rate of $20°.min^{-1,}$ an accelerating voltage of 40Kv, and a filament current of 40 mA. The crystallite size of NV was calculated through Scherrer equation ($D=k\lambda/(B\cos\theta)$. To clarify the binding modes of the surface elements, X-ray photoelectron spectroscopy (XPS) was measured through VG-microteach-multilab (ESCA-3000) fitted with non-monochromatized Cu-Kα-X-ray source (E=1253.6 eV). The binding energy was calibrated through C 1s photoelectron peak intensity at 284.6 eV as reference. High resolution transmission electron microscopy (HRTEM) was examined to investigate the crystallographic nanoscale structure and field emission scanning

electron microscopy (FESEM) with EDS (JEOL-JEM-2100) was inspected to find the elemental distribution of the morphology. The diffused spectral absorption properties of the synthesized photocatalyst were analysed utilizing JASCO-V750 UV-Vis spectrometer within the test range of 200-800 nm wavelength, and the spectral bandwidth was 0.1 nm. For analysis, first $BaSO_4$ was used as reference test material and the slit width was 5.0 nm. Similarly, the PL was carried out by JASCO-FP-8300 fluorescence spectrometer to record the photoluminescence spectroscopy at excitation wavelength=320 nm. Time resolution spectra (TRPL) were analysed through Edinburgh-FLS920 Fluorescence spectrometer with a multichannel scaling (MCS) module connected to F290H pulsed Xe μs flash light source. The functional group of semiconduction material are detected by Fourier transform infrared spectrometer (JASCO FT/IR-4600) from the 4000–400 cm^{-1} of wavenumber. Raman spectra were acquired by using a microlaser spectrometer equipped with laser of 545.5 nm. The textural properties include specific surface area was identified using Brunauer–Emmett–Teller (BET) N_2 adsorption–desorption isotherm technique at 77 K temperature (NOVA3000, Quanta chrome GmbH, Germany) and the pore size and pore volumes of the catalyst was calculated by the Barrett–Joyner– Halenda (BJH) technique.

Photoelectrochemical Characterisations Techniques

The photoelectrochemical characterisations were analysed using the IVIUM n STAT multichannel electrochemical analyzer, contains traditional three electrodes set-up connected with 300 W Xenon lamp attached with 420 nm cutoff filter. The complete analysis was carried out using 0.01M Na_2SO_4 electrolyte solution. The working electrode was prepared through drop casting method as follows. At first, 10 mg of prepared sample with 0.5 ml IPA and 20μl nafion solution was ultrasonically dispersed and after that the slurry of the photocatalyst was deposited on the conducting FTO surface. Pt was used as a counter electrode and Ag/AgCl was used as reference electrode. Mott-Schottky measurements were performed in the absence of light at a frequency of 1000 Hz. EIS measurement was conducted under visible light illumination across a frequency range of 10^7 to 10^{-1} Hz at an amplitude of 0.01 with zero bias. The LSV analysis was carried out under visible light, applying a potential range from 0.4-1.6 V with 10 mVs^{-1} scan rate. The transient photocurrent response (TPC) was recorded at 0.2 V. The photocurrent behaviour of all photocatalytic materials was evaluated through repeated on-off cycles over a 300-second duration, with 30-second intervals between each cycle.

Experimental protocol for photocatalytic Cr(VI) reduction and H_2O_2 Production

Initially, the photocatalytic ability of NV was analysed by photocatalytic Cr(VI) reduction at room temperature. In the experiment anhydrous $K_2Cr_2O_7$ (0.071g) was dissolved in 500 ml deionised water to prepare 25 ppm Cr(VI) stock solution. For the removal test, a 50 ml stock solution was taken with 10 mg of sample and continuously stirred for 30 minutes in dark to attain the adsorption-equilibrium. At certain time interval 2 ml of solution was taken from the beaker and filtered. The concentration of Cr(VI) and Cr(III) was determined using an ultraviolet visible Spectro photometer. 0.1 mol/L H_2SO_4 and 0.1 mol/L NaOH were used to adjust the pH solution. The Cr(VI) photoreduction was confirmed through colorimetric method, where 2 ml of supernatant solution was mixed with 2 ml of Sulfuric acid (3M) and 1 ml of fresh prepared solution of 1,5-diphenylhydrocarbazide (DPC). The adsorption kinetics were evaluated by measuring the change of solution concentrations at different times. The initial concentration of the solution was set to 20 mg/L.

Further the earlier prepared materials are examined for H_2O_2 photocatalytic generation. The analysis was done using NV samples in an photocatalytic reactor at ambient temperature. Each quartz tube in the reactor contained 20.0 mg of photocatalyst dispersed in 19.0 ml of deionized water with 1 ml of IPA via ultrasonication. Before light irradiation, the sample undergoes 40 minutes of stirring under oxygen purging, and then 2 hours of continuous stirring to establish adsorption-desorption equilibrium. Subsequently, under constant stirring (400 rpm) the NV sample solution was irradiated by a 250 W Mercury lamp ($\lambda \geq 420$ nm) for the photocatalytic production of H_2O_2. To observe H_2O_2 production over time, 4.0 ml of solution was tested at various intervals to analyse H_2O_2 concentration. After filtration of the NV photocatalysts, H_2O_2 concentration in the collected solution was determined using an iodometric method. This involved adding 50.0 µl of 0.4 M potassium iodide and 50.0 µl of 0.1 mM ammonium molybdate tetrahydrate to the 3.0 ml collected solution. The resulting colour solution was then analysed using UV-vis spectrophotometry at 350 nm. More in, the as-prepared photocatalysts were analysed for H_2O_2 production with different pH (3.0, 6.0 and 9.0), various proton donor (water, IPA, methanol and ethanol) and several atmospheres (O_2, N_2, Ar and air) through above mentioned procedure. To gain deeper understanding of the active species involved in the photocatalytic H_2O_2 production, $AgNO_3$ and CA were employed as scavengers for e^- and h^+, respectively, under light irradiation for 1 h in an O_2 saturated environment. In detail, 20 mL of DI along with 20 mg of photocatalyst and 1 mM of each scavenging agent was taken in an irradiation chamber. The solution was stirred in the dark for

30 minutes; it was exposed to visible light for 1 h. Then the sample was taken out and analysed.

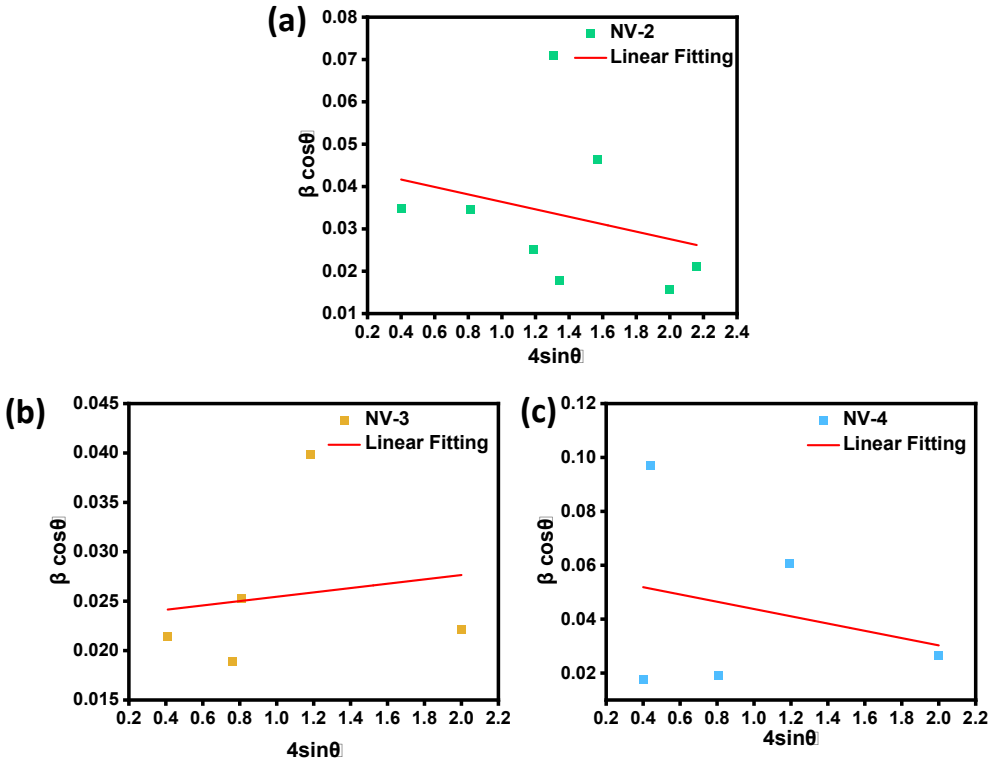

Figure S1. Williamson-Hall plot for (a) NV-2 (b) NV-3, and (c) NV-4

Table S1: Estimated crystallite parameter for (003) plane of NV photocatalysts

Sample	Average Crystallite size (D)	Average Lattice Constant(Å)	Micro strain (ε)	Interlayer spacing(d) (003)	Delocalization density $\delta=1/D^2$
NV-2	4.86	5.0399	33.19	7.6819	0.3389
NV-3	5.03	6.5659	30.65	7.6356	0.0396
NV-4	6.08	5.7110	70.77	7.5511	0.0271

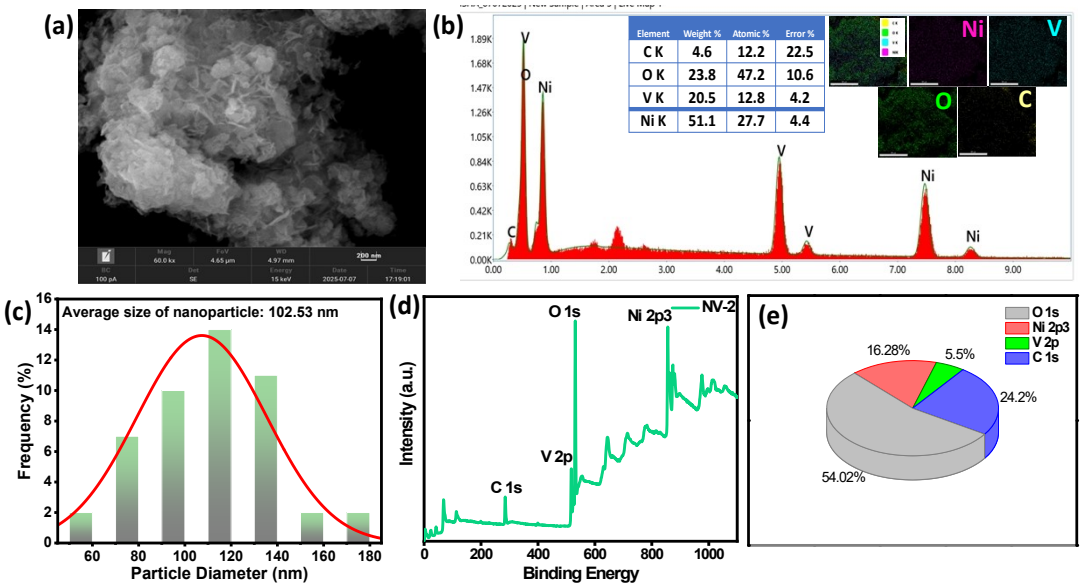

Figure S2. a) SEM micrograph b) EDX pattern c) Particle size distribution analysis d) XPS survey spectra e) Atomic percentage graph oh NV-2 photocatalyst

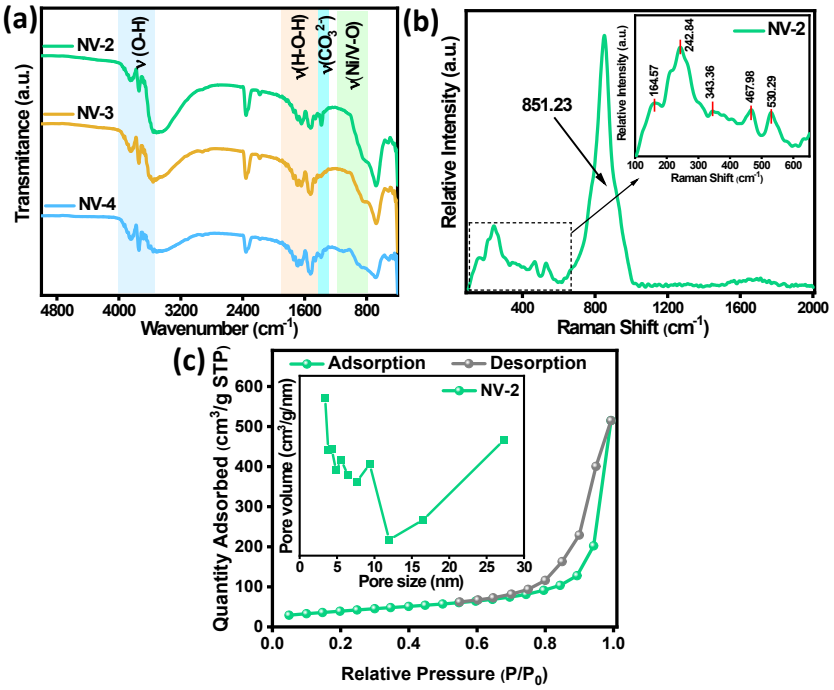

Figure S3.a) FT-IR spectra, b) Raman spectra and c) N_2 adsorption desorption plot of NV-2

The band gap value was accurately determined through linearly extrapolating the linear part of $(\alpha h\nu)^n$ curve to 0 by the following Eq. S1:

$$(\alpha h\nu)^n = A(h\nu - E_g) \text{----------(S1)}$$

in which α, ν, h, E_g and A refer to the absorption coefficient, light efficiency, Planck constant, band-gap energy and proportional constant, respectively.

Table S2: Estimated bandgap, and Urbach energy at calculated absorbance edge

Photocatalyst	Bandgap	Absorption maxima (λ in nm)	Absorbance edge (λ in nm)	Urbach energy
NV-2	1.58	345	580	0.876
NV-3	1.46	340	575	0.724
NV-4	1.23	330	587	0.605

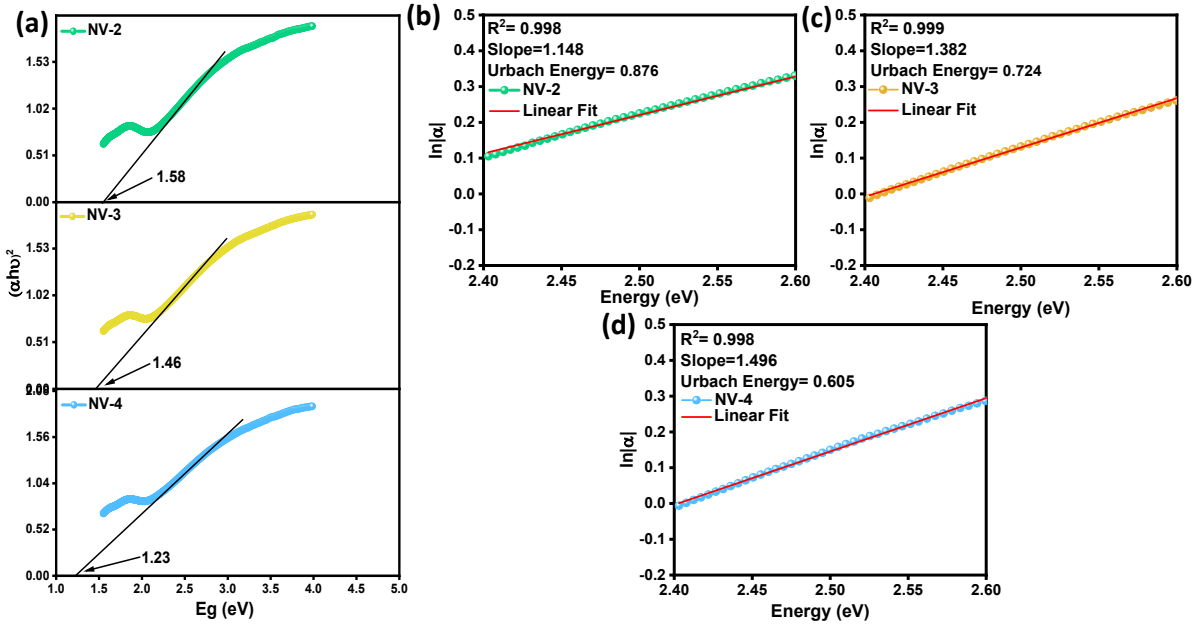

Figure S4. a) Tauc plot and Urbach Energy plot of b) NV-2, c) NV-3 d) NV-4

Biexponential function for TRPL fitting:

$$Fit = A + \propto_1 \exp\left\{\frac{-t}{\tau_1}\right\} + \propto_2 \exp\left\{\frac{-t}{\tau_2}\right\} \text{----------} (S2)$$

Where A is a constant, α_1 and α_2 are relative contributions and τ_1 and τ_2 are the decay lifetimes of the respective compounds.

Table S3. Lifespan of electrons derived from Bode phase plot

Sample ID	f_{max}	Electron life span (τ in μs)
NV-2	4003	39.8
NV-3	3006	52.9
NV-4	1753	90.8

Photocatalytic H_2O_2 decomposition

$$[H_2O_2] = {}^{K_f}/_{K_d} \times \{1 - \exp(-K_d t)\} \quad \text{(S3)}$$

$$K_d = -ln({}^{C_t}/_{C_0})/t \quad \text{(S4)}$$

Where K_f and K_d represents the zeroth- and first-order kinetic constants respectively and $[H_2O_2]$ is the concentration of H_2O_2.

Ct and Co are the concentration of H_2O_2 (μmol L^{-1}) at t and initial time, correspondingly.

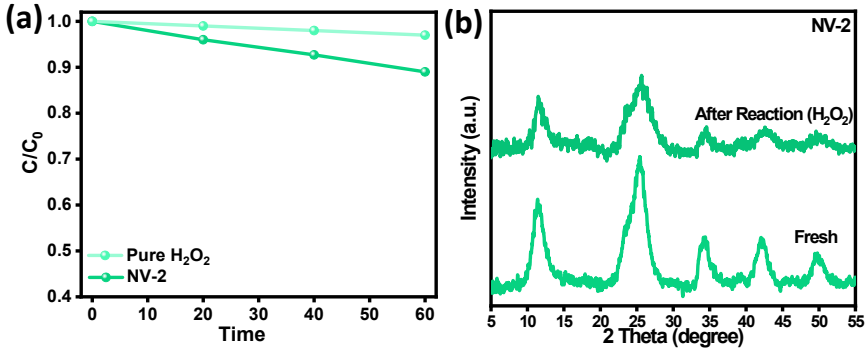

Figure S5. a) The photocatalytic decomposition of H_2O_2 under visible light irradiation of NV-2 photocatalyst. b) XRD pattern of NV-2 before reaction and after reaction

Table S4. Comparison of photocatalytic H_2O_2 productions by various photocatalytic system with our system

Sl No.	Materials	Sacrificial agent	Light source	H_2O_2 evolution (μmol h^{-1} g^{-1})	Ref.
1	MPa-COFs/CQDs	-	LED lamp (300 W, λ > 380 nm)	540	5
2	CN-QDs@MA	-	300 W Xenon	39.82	6

			lamp		
3	LYH/CQDs/AIS-3/IS	ethanol	300W Xenon lamp	902.9	7
4	FCCN	ethanol	300 W Xe lamp	224.24	8
5	CdSe/KPN-HCP	-	visible light	900.0	9
6	AgQDs/ZnO	-	visible light (λ >420 nm)	124	10
7	SN-GQD/TiO2	-	500 W Xenon lamp (λ ≥ 420 nm)	451	11
8	WS_2/Sulfur-Dopedg-C_3N_4	IPA	visible light (λ＞250 nm)	817	12
9	OE-CQD	-	150 W Xenon arc lamp	356.86	13
10	NV-2	IPA	250W Hg lamp	1152	This Work

Table S5. Comparison of photocatalytic Cr(VI) reduction by various photocatalytic system with our system

Sl No.	**Materials**	**Cr (VI) reduction (%)**	**Ref.**
1	Ni/Al@PAB	80	14
2	MgAl–bentonite comp.	70	15
3	Mg-Al LDH	78.54	16
4	Ti_3AlC_2	72.84	17
10	NV-2	81.5	This Work

Solar to chemical conversion efficiency (SCC %):

SCC % of NV-2 photocatalyst towards H_2O_2 generation under 250 W Hg-lamp can be calculated by the following equation:

$$SCC\% = \frac{\Delta G^{\circ} for\ H_2O_2\ generation\left(J/_{mol}\right) * H_2O_2\ produced\ (mol)}{Input\ energy\ (W) * reaction\ time\ (sec)} * 100 \ldots\ldots\ldots (S5)$$

Further, for H_2O_2 evolution is ΔG° 117 kJ·mol^{-1}. The irradiance of 250 W Hg-lamp is 1.33 W cm^{-2} and irradiated area is 36.2 cm^2 (3.14 × (3.4)^2 cm^2).

Input Energy (W) = $irradiance\ (Wcm^{-2}) \times irradiated\ area\ (cm^2)$

= 48.1 W

Acc. to equation (S5), the SCC efficiency is calculated to be 0.089 %.

Reference

1) K. Parida, L. Mohapatra, Recent progress in the development of carbonate-intercalated Zn/Cr LDH as a novel photocatalyst for hydrogen evolution aimed at the utilization of solar light. *Dalton Trans.* 2012, **41**,1173-1178.
2) N. Baliarsingh, L. Mohapatra, K. Parida, . Design and development of a visible light harvesting Ni–Zn/Cr–CO_3^{2-} LDH system for hydrogen evolution. *J. Mater. Chem. A.* 2013, **1**, 4236-4243.,
3) A. Sherryna, M. Tahir, Z.Y. Zakaria, Trimetallic $Ni_xCo_yAl_z$ LDH-Modified g-C_3N_4 with Influential Effects of M^{2+}/M^{3+} (Ni/Co) Active Centers for Stimulating Photocatalytic Hydrogen Production. *ACS Appl. Energy Mater*, 2024, **7**, 6289-6311.
4) P.P. Sarangi, K.K. Das, J. Sahu, U.A. Mohanty, D.P. Sahoo, K. Parida, Structurally Modulated NiV-LDH with CdMoSe-Quantum Dots: Unlocking the Active Centers at S-Scheme Heterojunctions for Stimulating Photocatalytic H_2O_2 Production and H_2 Evolution, *Inorg. Chem.*,2025, **64**, 2723-2736.
5) Y. Cong, X. Li, S. Zhang, Q. Zheng, Y. Zhang, S.W. Lv, Embedding carbon quantum dots into crystalline polyimide covalent organic frameworks to enhance water oxidation for achieving dual-channel photocatalytic H_2O_2 generation in a wide pH range. *ACS Appl. Mater. Interfaces.* 2023, **15**, 43799-43809.
6) M. Yin, X. Chen, Y. Wan, W. Zhang, L. Feng, L. Zhang, H. Wang, Doping carbon nitride quantum dots into melamine-silver matrix: an efficient photocatalyst with tunable morphology and photocatalysis for H_2O_2 evolution under visible light. *ChemCatChem*, **2020**, *12*,1512-1518.

7) K. Zhang, M. Zhou, K. Yang, C. Yu, P. Mu, Z. Yu, K. Lu, W. Huang, W. Dai. Photocatalytic H_2O_2 production and removal of Cr (VI) via a novel Lu_3NbO_7: Yb, Ho/CQDs/AgInS2/In2S3 heterostructure with broad spectral response.*J. Hazard. Mater.* 2022, **423**,127172.

8) M. Zhang, C. Lai, B. Li, F. Xu, D. Huang, S. Liu, L. Qin, Y. Fu, X. Liu, H. Yi, Y. Zhang, Insightful understanding of charge carrier transfer in 2D/2D heterojunction photocatalyst: Ni-Co layered double hydroxides deposited on ornamental g-C3N4 ultrathin nanosheet with boosted molecular oxygen activation. *Chem. Eng. J.* 2020, **396**, 125343.

9) J. Xu, Q. Ji, Y. Wang, C. Wang, L. Wang, enhanced photocatalytic H_2/H_2O_2 production and tetracycline degradation performance of CdSe quantum dots supported on K, P, N-co-doped hollow carbon polyhedrons, *Chem. Eng. J.* 2021, **426**, 130808.

10) C. Zhang, F. Zhou, S. Zhan, Y. Song, F. Wang, J, Lai. The enhanced photocatalytic inactivation of marine microorganisms over ZnO supported Ag quantum dots by the synthesis of H_2O_2. *Environ. Res.* 2021, **197**, 111129.

11) L. Zheng, H. Su, J. Zhang, L.S. Walekar, H.V. Molamahmood, B. Zhou, M. Long, Y.H, Hu. Highly selective photocatalytic production of H_2O_2 on sulfur and nitrogen co-doped graphene quantum dots tuned TiO_2. *Appl. Catal., B.* 2018, **239**, 475-484.

12) K. K. Das, U. A. Mohanty, R. Mohanty, P. P. Sarangi, D. P. Sahoo, K. Parida, Improving charge carrier separation through S-scheme-based 2D–2D WS_2/sulfur-doped g-C_3N_4 heterojunctions for a superior photocatalytic O_2 reduction reaction. ACS Appl. Energy Mater. 2024,**7**,6360−6375.

13) D.Y. Lee, Z. Haider, S.K. Krishnan, T. Kanagaraj, S.H. Son, J. Jae, J.R. Kim, P.S.M. Kumar, H.I Kim. Oxygen-enriched carbon quantum dots from coffee waste: extremely active organic photocatalyst for sustainable solar-to-H_2O_2 conversion. *Chemosphere*, 2024, **361**, 142330.

14) Tran, H.N.,. *Chem. Eng. J.*, **2019**, *359*,810-812.

15) M. De Geest, B. Michielsen, R.G. Ciocarlan, P. Cool, E.M. Seftel. Structured LDH/bentonite composites for chromium removal and recovery from aqueous solutions. *Molecules*, 2023, **28**, 4879.

16) B. Zeng, Q. Wang, L. Mo, F. Jin, J. Zhu, M. Tang, Synthesis of Mg-Al LDH and its calcined form with natural materials for efficient Cr (VI) removal. *J. Environ. Chem. Eng*, 2022, **10**, 108605.

17) Q. Yang, X. Bao, Z. Li, A. Yang, Y. Cao, X. Hu, L. Yu, B. Liu, Visible-light-enhanced Cr (VI) reduction and bioelectricity generation at MXene photocathode in photoelectrocatalytic microbial fuel cells, *J. Water Process Eng*, 2022, **45**, 102454.